Chapter 7

Magnetic Properties of Hausmannite Thin Films

Petya Petkova

Additional information is available at the end of the chapter

http://dx.doi.org/10.5772/66533

Abstract

The magnetic properties of hausmannite thin films are investigated in this chapter. The Verdet constant and angle of Faraday rotation are determined. The magnetic anisotropy of Mn_3O_4 is explained by the measurement of the zero-field cooled (ZFC) and field cooled (FC) curves. This experiment is connected with the presentation of the ferromagnetic to superparamagnetic transition of the hausmannite.

Keywords: hausmannite Mn_3O_4, Faraday effect, verdet constant, ferromagnet, superparamagnet

1. Introduction

The hausmannite Mn_3O_4 can be fabricated by many methods, but the spray pyrolysis method can give it the highest quality. This material is very interesting because it is a transition metal oxide and has application in semiconductor devices [1]. This oxide has two valance states on manganese—Mn^{2+} and Mn^{3+}. Thus, spinel Mn_3O_4 occurs in nature as the mineral hausmannite [$Mn^{2+}Mn_2{}^{3+}O^4$]. The Mn^{2+} cations occupy the tetrahedral sites and Mn^{3+}cations occupy the octahedral sites [2]. The nanoparticles of Mn_3O_4 thin film behave as single-domain ferromagnets. However, above the blocking temperature, the particles behave as paramagnets due to the dominance of thermal fluctuations over the magnetocrystalline anisotropy energy. These nanoparticles have much higher magnetic moments than other paramagnets and are called superparamagnet.

The detailed investigation of magnetic properties of hausmannite thin film is presented in this chapter.

2. Method of preparation and characterization techniques

Several techniques have been used to prepare thin films of these types of transparent and conductive materials to meet the requirements of search and industries such as MOCVD (organometallic chemical vapor deposition) [3], chemical vapor transport (CVT) [4], sputtering [5] and laser ablation [6, 7], which are generally either sophisticated or expensive and hence the need for a simple, easy to meter out and less expensive technique. In addition to these techniques, spray pyrolysis [8–11] has received a little bit of extra attention because of its simplicity and cost-effectiveness as it does not require sophisticated vacuum apparatus. Furthermore, this method can be selected for film production of large area with size grain controllable by controlling the doping concentration. Also, this technique leads to a large production area and it permits also the formation of thin films with possible control of oxygen vacancy by means of the use of both appropriate precursors and postannealing treatments in air [12–15].

Thin films of Mn_3O_4 were grown at 350°C on 1 × 2 cm^2 glass substrate using the spray pyrolysis technique. The substrate temperature was fixed using a digital temperature controller with a k-type thermocouple. The aqueous solution with a flow of about 4 ml/min contains magnesium chloride ($MnCl_2.6H_2O$) 0.1 M as precursor. The distance between the nozzle and the substrate was about 27 cm. Spray solutions quantity (75 ml) was kept fixed during the growth. The filtered compressed nitrogen air was used as gas carrier at a flow of 4 l/min. The total deposition time was maintained at 20 min. After deposition, the coated substrates were allowed to cool down naturally to room temperature (**Figure 1**).

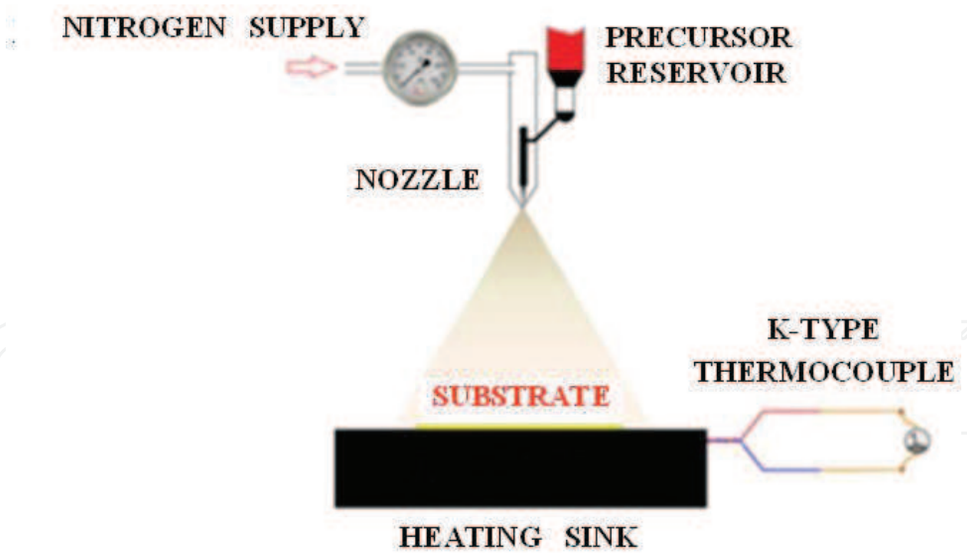

Figure 1. The experimental set up for the spray pyrolysis technique.

The crystalline structure was analyzed by X-ray diffraction, using a Siemens D500 diffractometer with monochromatic CuKα radiation (λ = 1.54 Å) [16]. The surface morphology of the Mn_3O_4 thin film is further analyzed using atomic force microscope (AFM) using a Veeco digital

instrument 3 A microscope. The sample was probed in a tapping mode with a nanometer scale.

3. Magnetic study

The magneto-optic Faraday effect presents the connection between optics, magnetism and atomic physics. Faraday rotation manifests itself as a rotation of the polarization plane of the light passing through the sample in the presence of a magnetic field and is characterized by the Verdet constant (V) of the investigated sample (**Figure 2**). The rotation angle φ can be expressed by the formula [17]:

$$\varphi(\lambda) = A/(\lambda^2 - \lambda_0{}^2), \tag{1}$$

where A is a constant determined from the matrix elements of the interband transitions, λ is the wavelength and λ_0 is the wavelength related to the interband transitions and corresponding to the natural frequency $\omega_0 = 2\pi/\lambda_0$ of an effective harmonic oscillator. The relationship between the rotation angle and the Verdet constant is φ = VBl, where B is the magnetic induction of the field and l is the sample thickness (**Figure 3**). The magneto-optic anomaly factor γ (**Figure 4**) can be taken as a measure of the degree of covalency that exists in the bonds connecting the ions and atoms [18]:

$$\gamma = \frac{\varphi}{\frac{e}{2mc^2}\lambda D} \tag{2}$$

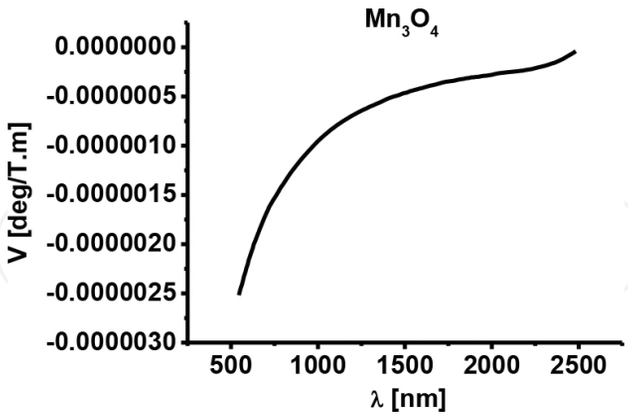

Figure 2. The Verdet constant for Mn_3O_4 in the spectral region 500–2500 nm.

In the paramagnetic materials, the anomaly factors γ can vary with the wavelength of the incident light, even if there is only one absorption frequency contributing to dispersion. The dispersivity of the investigated crystal can be presented by the following equation:

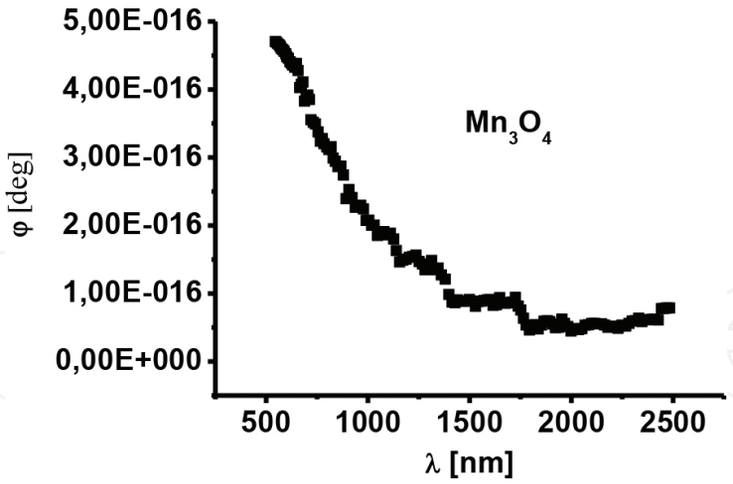

Figure 3. The Faraday rotation angle as a function of the wave length (500–2500 nm) for Mn_3O_4 thin film.

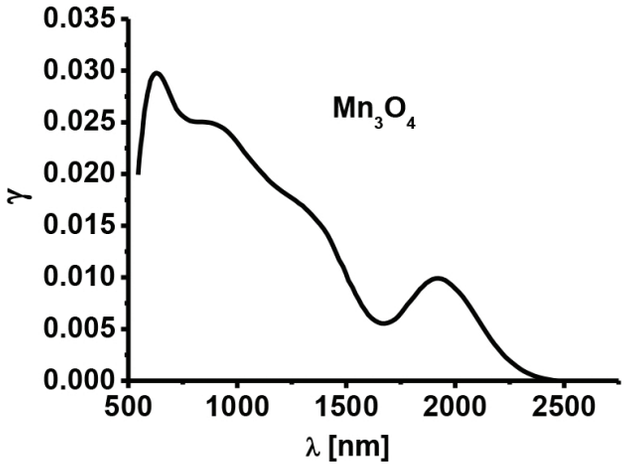

Figure 4. The magneto-optic anomaly factor γ for hausmannite in the spectral region 500–2500 nm.

$$D = -\frac{\gamma}{c}\frac{d^2n}{d\lambda^2}. \tag{3}$$

$$\gamma = -\frac{VBl}{\frac{e\lambda^2}{2mc^2}\frac{d^2n}{d\lambda^2}}. \tag{4}$$

The spectral dependence of the spin-spin exchange interaction constant K in the case of Mn_3O_4 thin film is presented in **Figure 5**. It can be calculated by the following formula [19]:

$$K(\lambda) = \frac{V\left[\left(\left(\frac{\lambda}{\lambda_g}\right)^2 - 1\right)\right]^{3/2}}{\chi^{\lambda}}, \tag{5}$$

where V is the Verdet constant, χ is the magnetic susceptibility of the sample (**Figure 6**) and λ_g represents the band gap of the material. For the investigated vanadium doped crystal

λ_g = 556 nm [16]. When the spin-spin exchange interaction constant has negative values, the spins align antiparallel to each other so that the net magnetization is zero. Therefore, the material is antiferromagnet and it is modeled to be made up of two sublattices [20].

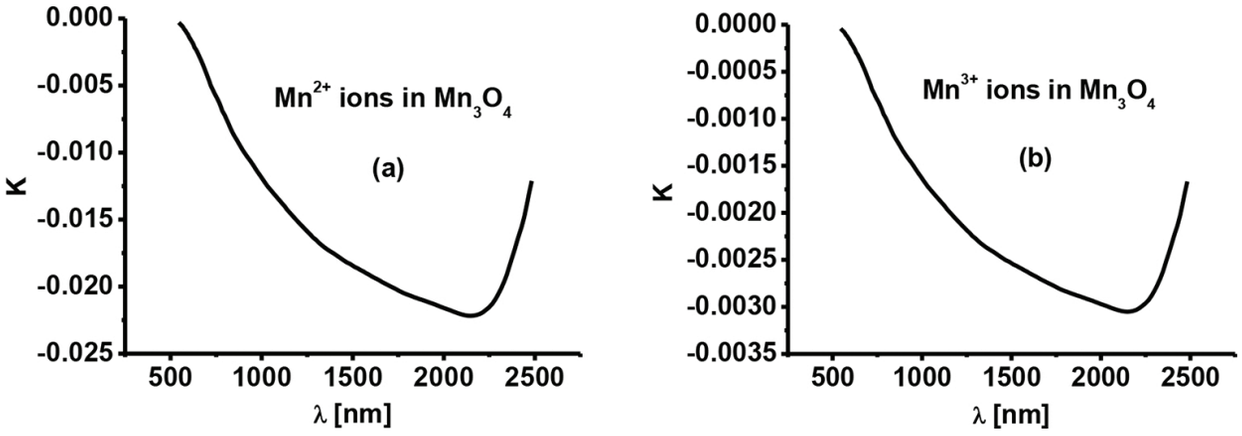

Figure 5. The constant of spin-spin exchange interaction $K(\lambda)$ for Mn^{2+} (a) and Mn^{3+} (b) in Mn_3O_4 thin film (500–2500 nm).

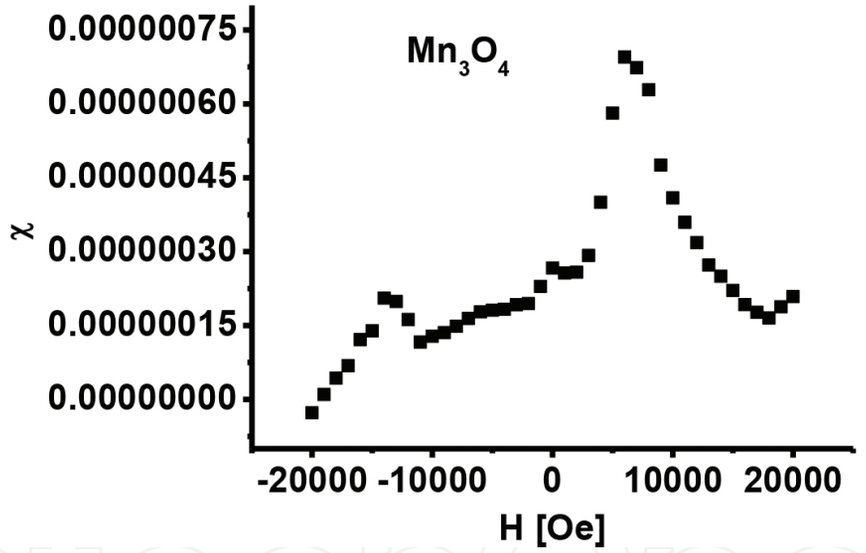

Figure 6. The dependence $\chi(H) = dM/dH$ for Mn_3O_4 in the magnetic field from −20,000 to 20,000 Oe.

The exchange interaction energy leads to the alignment of neighboring atomic moments and this forms magnetic domains. The magnetostatic interaction energy tries to break them into smaller domains oriented antiparallel to each other. The domain size depends on the relative counterbalance between both energies. The system is composed of a single domain, when the magnetostatic energy does not allow the breaking of domains into smaller parts. This condition is connected with the critical value r_c of the radius of a spherical particle. If the rotation of the atomic magnetic moments is coherent (the structure is a single-domain one), then the particle can be characterized by its total magnetic supermoment $|\vec{\mu}_p| = M_S V$, where V is the particle volume and M_S is saturation magnetization. The ferromagnetism and super paramagnetism are observed, respectively, below and above the blocking temperature T_B. Its origin is

connected with magnetic anisotropy within particles. This anisotropy tends to orientate the particle supermoment along some preferential direction.

The spin-orbit coupling and dipolar interaction dictate preferential orientation directions of the magnetic moments because of the finite size of the particles. The magnetic anisotropy energy E_A of the particles can be described by a simple model. This model includes two main contributions: crystalline and shape, which are connected with the core and surface atoms, respectively. When the particles are spherical and the anisotropy is uniaxial crystalline, the considered situation is the simplest [21]. If the magnetic anisotropy is proportional to the particle volume, then $\vec{K}_{\text{eff}} = KV\hat{n}$, where K is the effective uniaxial anisotropy constant (per unit volume) and $\hat{n}$ is the unitary vector describing the easy-magnetization anisotropy. The energy term for the i particle can be written as:

$$E_A^{(i)} = -K_i V_i \left(\frac{\vec{\mu}_i \cdot \hat{n}_i}{|\vec{\mu}_i|} \right)^2 = -K_i V_i \cos^2\theta, \tag{6}$$

where θ_i is the angle between the magnetic supermoment of the particle and the easy anisotropy axis (**Figure 7**). The moment of the particle has therefore two preferred orientations, energetically equivalent, along the easy-magnetization anisotropy axis direction. Both directions are separated by an energy barrier E_B of height $K_i V_i$.

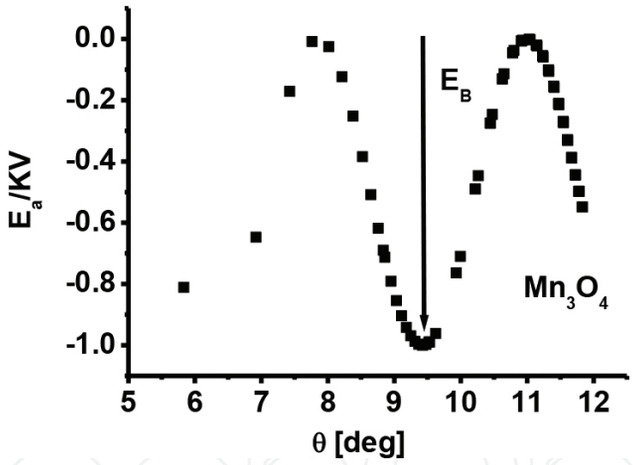

Figure 7. Schematic drawing of the ideal simplest model of noninteracting and parallel aligned easy axes along the applied field.

If the particles are magneto anisotropic, the calculation of equilibrium magnetization is complicated. The special role for nanoparticles having superficial anisotropy is the violation of local symmetry surroundings and crystal field change that acts on the magnetic ions from the surface. The simplest type of magnetic anisotropy is the easy anisotropy axis.

When external magnetic field is applied over the nanoparticles, it tries to orientate their magnetic moments in the direction of its action. Therefore, if the magnetic field is applied perpendicular of anisotropy axis and the orientation of magnetic moment of the particle is labeled with i, the next equation is fulfilled:

$$E^i = E_A^{(i)} + E_Z^{(i)} = -K_i V_i \left(\frac{\vec{\mu}_i \hat{n}_i}{|\vec{\mu}_i|} \right)^2 - \vec{\mu}_i . \vec{H}, \tag{7}$$

where E_A and E_Z are Zeeman energies.

The influence of external magnetic field in the orientation of magnetic supermoments is known as Stoner-Wohlfart model [22]. They assume that the coherent rotation of atomic magnetic moments exists and the magnetic field is applied at a certain angle θ_0 with respect to the easy anisotropy axis. When the temperature effects are ignored the problem can be solved with minimal number of energetic arguments. The situation is very interesting, when we can describe the change of magnetic moments in dependence of anisotropic energy barrier and the temperature T_B. This is the reason for the study of a simple case when the field is applied parallel to the easy anisotropy axis. It should also be noted that the particles are identical and do not interact with each other. The application of the field leads only to their arrangement in the direction of the easy anisotropy axis. Thus, the following equation can be written (**Figure 8**):

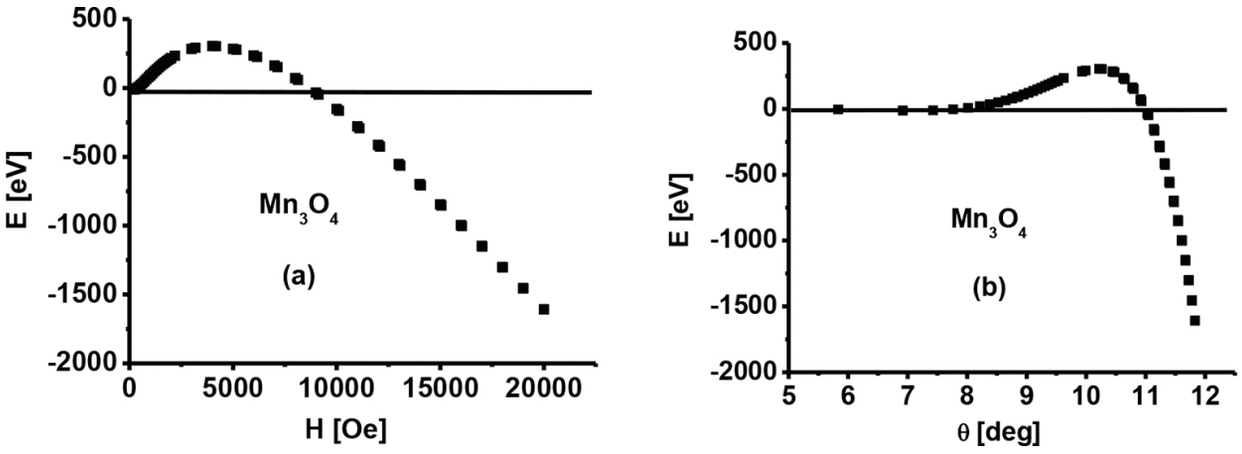

Figure 8. The dependence of anisotropic energy barrier from the external magnetic field (a) and the angle between the applied field and easy anisotropy axis (b).

$$E = -KV\cos^2\theta - M_S VH\cos\theta \tag{8}$$

when $H < 2K/M_S$, Eq. (8) gives two local minima (the directions of easy magnetization) at $\theta = 0$, π with values $E_{\min} = -KV \pm M_S VH$ (**Figure 9**) and one maximum (the direction of hard magnetization) at $\theta = \arccos(HM_S/2K)$, with value $E_{\max} = KV(HM_S/2K)^2$. The direction of hard magnetization is perpendicular of the anisotropy axis in the case, when $H = 0$. The value $\theta = 0$ is valid, when the moment of particles is oriented parallel to the magnetic field (↑↑). The equation $\theta = \pi$ is fulfilled when the orientation of the moment of the particles is antiparallel to the magnetic field (↑↓). The difference between the shapes of the energy wells is connected with the different energy barriers. These barriers depend on the orientation of the moments of particles to the applied field which can be written as $E_B^{\uparrow\downarrow}$ and $E_B^{\uparrow\uparrow}$ for the cases of antiparallelism and parallelism, respectively.

The anisotropy field of the particles is introduced as $H_A = 2K/M_S$. The energy barriers can be calculated as the difference between the minimal and maximal energies: $E_B^{\uparrow\downarrow} = \frac{KV}{H_A^2}(H-H_A)^2$ and $E_B^{\uparrow\uparrow} = \frac{KV}{H_A^2}(H+H_A)^2$ (**Figure 10**). The difference between the heights of energy barriers also shows a change in the characteristic time for relaxation of the particles, since it depends on the relative orientation of the magnetic dipoles to the field: antiparallel oriented particles have smaller energy barrier in comparison with the particles which are oriented along the easy anisotropy axis. They have also small heat energy sufficient to overcome the barrier. The parallel oriented particles are limited by deeper anisotropy well and the jump of their magnetic moments requires higher heat energy. When the particle has to rotate its magnetic moment, the energy of jump beyond the energy barrier is $E_B \approx KV$. The characteristic time of heat fluctuations of the magnetic moments can be presented by the formula [23]:

$$\tau = \tau_0 \exp(E_B/k_B T), \tag{9}$$

where $E_B/k_B T \geq 1$.

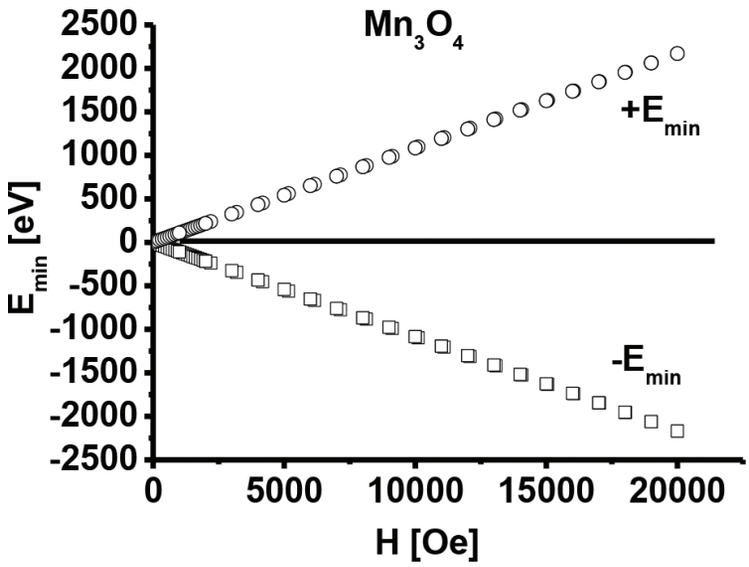

Figure 9. The local minimal energy $\pm E_{min}(H)$ in the directions of easy magnetization for the hausmannite Mn_3O_4.

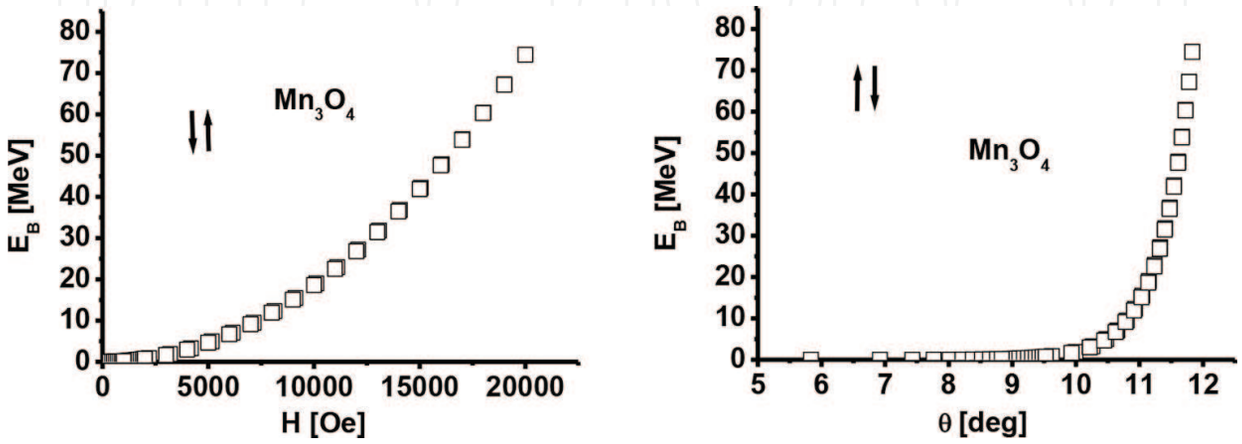

Figure 10. The dependence of the energy barriers E_B of: applied magnetic field and angle θ in the case of antiparallelism.

The multiplier τ_0 depends on many parameters such as temperature, gyromagnetic ratio, saturation magnetization, anisotropy constant and the size of the energy barrier. It is of the order of 10^{-9} – 10^{-13} s [24]. The formula (9) determines the characteristic time of establishing heat equilibrium in the system of noninteracting single-domain magnetic particles. At high temperatures, the following inequality is fulfilled: $E_B/k_BT \ll 1$. Therefore, the time of transition of the system in the state with minimal energy is small in comparison with the characteristic time of measurement τ_m. In this case, the system should not appear magnetic hysteresis. When $E_B/k_BT \gg 1$, the time of transition of a system in the equilibrium state depends on the size of the particles. If $\tau_m > \tau$, the system is in the super paramagnetic state and it quickly reaches equilibrium magnetization, when the temperature or the external field change. In the opposite case, when the external magnetic field changes, the system does not fail to relax in the new equilibrium state for the time τ_m and its magnetization does not change. The case when $\tau_m = \tau$ is connected with the blocking temperature:

$$T_B = \frac{KV}{25k_B}. \tag{10}$$

Formula (10) presents the temperature T_B, when the magnetic field is zero. This temperature decreases with the increasing of the external magnetic field by the law:

$$T_B(H) = T_B(0)\left(1-\frac{H}{H_c}\right)^k, \tag{11}$$

where $k = 2$ for small fields and $k = 2/3$ for big fields and $H_c = \frac{2k}{M_S}$.

The magnetization curve increasing to reaching saturation magnetization is measured in the study of the magnetic properties of the hausmannite Mn_3O_4 which containing nano-objects. To determine the temperature dependence of the magnetic moment Mare carried out two types of measurements—cooling in zero magnetic field (zero-field-cooling, ZFC) and cooling in a nonzero field (field-cooling, FC). The sample is cooled (to liquid helium temperature) during the method of ZFC in the absence of a magnetic field and then a small field (2–5 kOe) is included. The temperature values begin slowly to increase and the magnetic moment (M_{ZFC}) values can be registered. The technique FC differs from ZFC only by the fact that a sample is cooled in a nonzero magnetic field. The curves $M_{ZFC}(T)$ and $M_{FC}(T)$ for the magnetic nano-objects coincide at sufficiently high temperatures, but they begin to vary below a temperature T_H (irreversibility temperature). The curve $M_{ZFC}(T)$ has a maximum at a certain temperature T_{max} and it increases monotonically down to very low temperatures (**Figure 11**). The dependence of the magnetization from the applied field at two various temperatures is shown in **Figure 12(a)** and **(b)**. For an idealized system containing similar nanoparticles with uniaxial anisotropy and random orientation of easy magnetization axis, the difference of the temperature dependence $M_{ZFC}(T)$ and $M_{FC}(T)$ at a qualitative level follows from Eq. (8). In the case of zero field during the cooling below the blocking temperature, the magnetic moments of the particles are oriented along their axes of easy magnetization ($\theta = 0$ in Eq. (8)). The total magnetic moment of the system is zero in the beginning and in the end of the cooling process. The magnetic moments for which $\theta < 90°$ (see Eq. (8)) it is not necessary to overcome the

energy barrier, when the external field H is included. Therefore, they turn to a position with minimum energy, creating a nonzero magnetization of the system. In contrast, the magnetic moments for which the external field is included ($\theta > 90°$) are separated from the minimum energy of the potential barrier. They can overcome only this barrier for a very long time (see Eq. (9)). Therefore, in the case of ZFC measurements ($T < T_B$), the system is in a metastable state with a small total magnetic moment $\frac{M_S^2 H}{3k_V}$, which does not depend on the temperature.

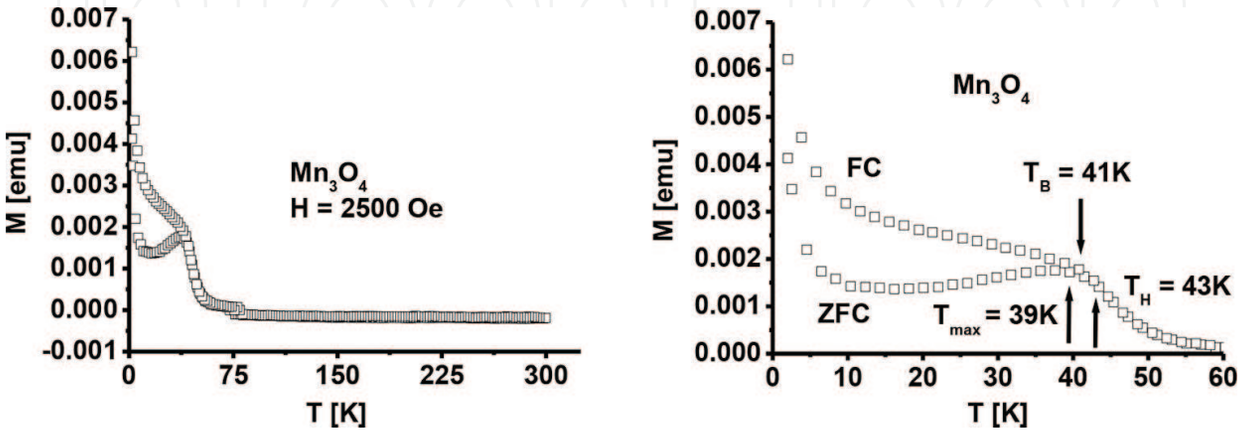

Figure 11. FC and ZFC induced magnetization as a function of temperature measured in a 2500 Oe field.

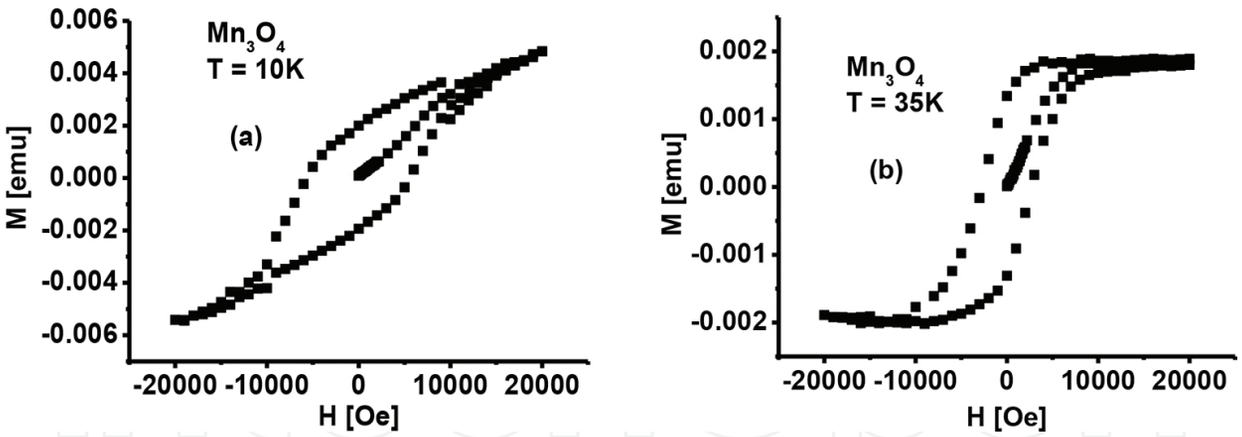

Figure 12. The magnetization $M(H)$ of hausmannite thin film for two temperatures $T = 10$ K (a) and $T = 35$ K (b).

At $T = T_B$, the system jumps into a stable superparamagnetic state with magnetic moment

$$M_{ZFC} \approx \frac{M_S^2 VH}{3k_B T} \tag{12}$$

When $M_S VH \ll k_B T$ and random orientation of the easy magnetization axes of particles, formula (12) is also valid for $T > T_B$. The sample is cooled in a nonzero magnetic field during FC

measurement and the magnetization at temperatures above T_B is determined by formula (12). At $T < T_B$, the system cannot change its magnetization during the measurement. Therefore, the magnetic moment which is determined by the FS method for $T < T_B$ is

$$M_{\mathrm{ZFC}} \approx \frac{M_S^2 VH}{3k_B T} = \text{const.} \tag{13}$$

The curves $M_{\mathrm{ZFC}}(T)$ and $M_{\mathrm{FC}}(T)$ are not separated at $T = T_B$ for a system consisting of a single-domain nanoparticles with dispersion of the size, the shape, etc. Their separation realizes at a higher temperature $T_H > T_B$, where T_H is called the irreversibility point. Another characteristic point on the curve $M_{\mathrm{ZFC}}(T)$ is the temperature $T_{\max}$ which is often equated with the average blocking temperature of the system $<T_B>$. At temperatures below $<T_B>$ we can observe the increase of $M_{\mathrm{FC}}(T)$ that replaced section "saturation" and sometimes we can observe a maximum [25]. The value of T_H can be identified with the blocking temperature for the particles with a maximum size and the temperature $T_{\max}$ corresponds to a blocking temperature for particles with minimum size. However, all of these characteristic temperatures (as well as their relationship with the particle size distribution by volume) may depend on the cooling rate and the subsequent heating of the sample. The intensity of the interaction between the particles also influences on the characteristics temperatures. If the heating rate of the sample is much smaller than its cooling rate, a maximum may be formed on the curve $M_{\mathrm{FC}}(T)$ at $T < <T_B>$ [26].

Note that the difference between the curves $M_{\mathrm{ZFC}}(T)$ and $M_{\mathrm{FC}}(T)$ is not observed only in systems of magnetic nano-objects, but also in macroscopic magnets with disorder elements (frustration of exchange bonds, topological disorder, structural defects) and even in ordered ferromagnets with a large magnetic anisotropy. The difficulties of theoretical research of the magnetic hysteresis in nano-objects consist in the fact that the phenomenon is nonlinear, nonequilibrium and nonlocal and it is caused by the existence of energy minima (due to the magnetic anisotropy) and separated barriers which have complicated dependence of the external magnetic field. The results of theoretical studies of simple models rarely give an acceptable description for real magnetic nanomaterials since their microstructure do not account, in particular, the influence of boundaries and defects on the local magnetization is not taken into account. The ferromagnetic-to-superparamagnetic transition of the hausmannite particles in the zero-field cooled (ZFC) and field cooled (FC) curves is presented in **Figure 8**.

The orientation of electron spin in the manganese ions is very interesting for study. One of the electrons of the inner shell is responsible for the magnetism and its spin is oriented upwards. If the conductivity electrons move in the same region, where there is the motion of "magnetic" electrons than their spins rotate in the opposite direction. Thus, the conductivity electrons can rotate the electron spins of the other ions. This double interaction is equivalent of the interaction between two "magnetic" electrons which are oriented in one direction. This means that the neighboring spins have to be parallel, which is a result from the action of intermediate environment. This mechanism does not require all electrons to be oriented upwards. It is sufficient that conductivity electrons can be slightly oriented downwards. Thus, the possibility for the rotation of "magnetic" electrons upwards increases.

The energy of electron spin can be presented as (**Figure 13**):

$$x = |\mu|\left(H + \frac{\lambda M}{\varepsilon_0 c^2}\right), \tag{14}$$

where $\mu = 2.8363*10^{-4}$ eVT^{-1}, $\lambda = 5700$ m^{-1}, $\varepsilon_0 = 8.8542*10^{-12}$ Fm^{-1} and $c = 8*10^8$ m/s (**Figure 13**).

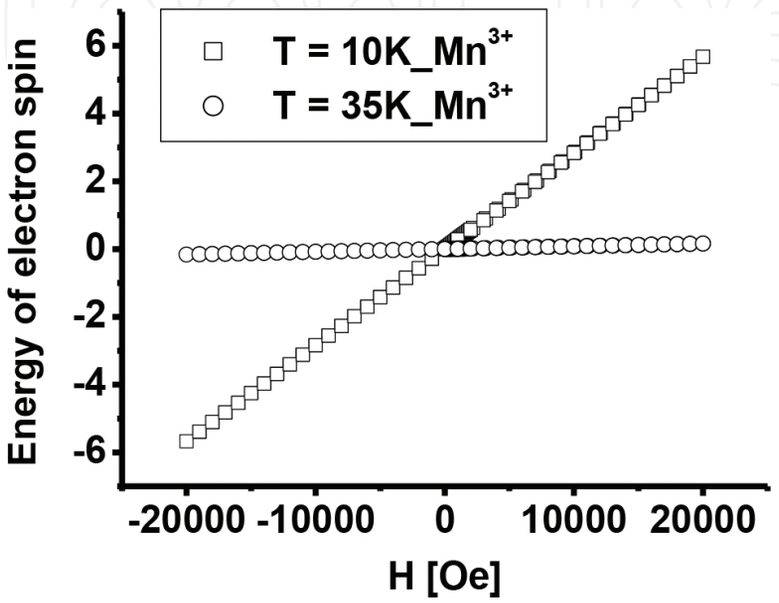

Figure 13. The energy of electron spin x as a function of the intensity of magnetic field H for Mn^{3+} ions at temperatures T = 10 K and T = 35 K.

On the other hand, we can write that

$$x = |m|(H + dM/\varepsilon_0 c^2)/kT, \tag{15}$$

where $d = 2.2971 \times 10^{-10}$ m.

The magnetic moment of the electron is

$$|m| = \frac{|\mu|\left(H + \frac{\lambda M}{\varepsilon_0 c^2}\right)}{(H + dM/\varepsilon_0 c^2)/kT} = 2.444110^{-7}, \tag{16}$$

where $k = 8.6173 \times 10^{-5}$ eVK^{-1}:

$$thx = th[|m|(H + dM/\varepsilon_0 c^2)/kT] \tag{17}$$

The energy of interaction between two electrons is expressed by the next equation (**Figure 14**):

$$\langle U \rangle = -N|\mu|\left(H + \frac{M}{2\varepsilon_0 c^2}\right) thx \tag{18}$$

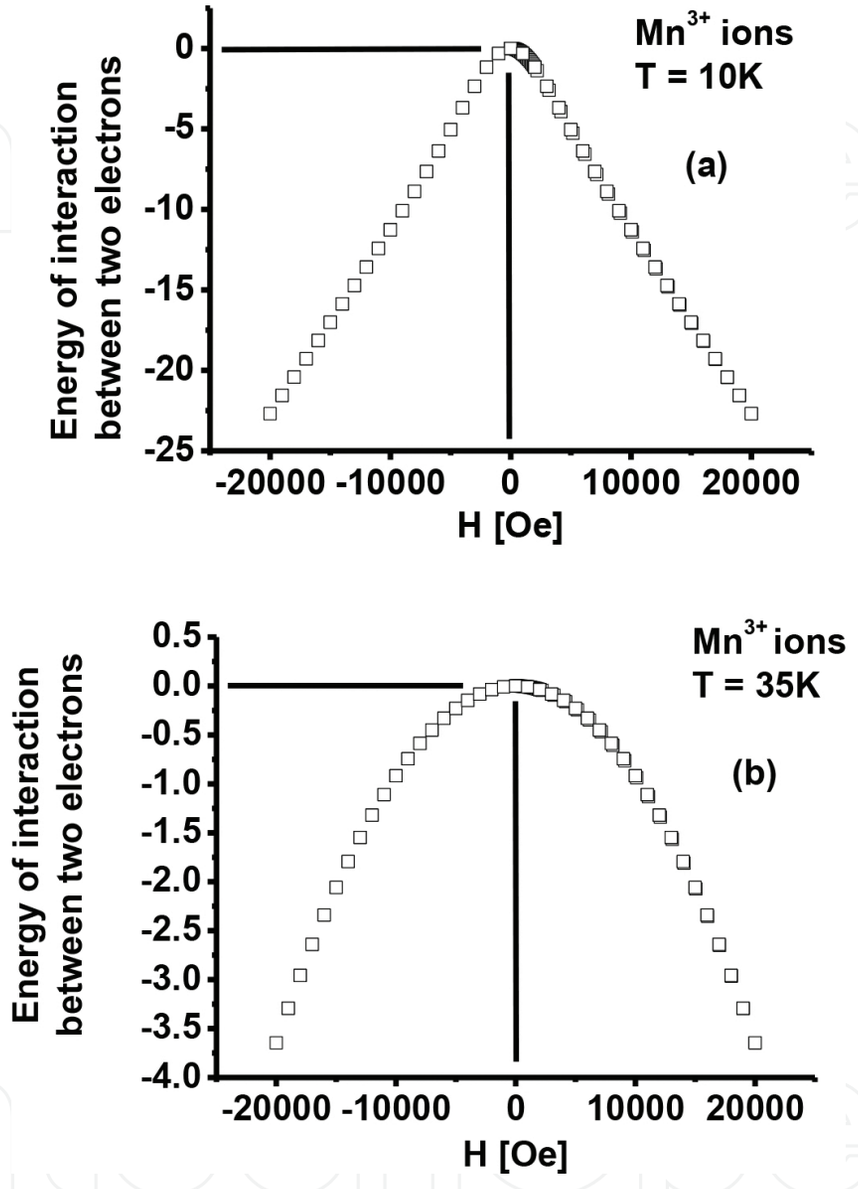

Figure 14. The average value of the energy of interaction between two electrons in Mn^{3+} ions as a function of the intensity of magnetic field H: (a) T = 10 K and (b) T = 35 K.

4. Conclusions

The magneto-optic anomaly factor γ for the hausmannite thin films decreases with the increasing of the wave length. The spin-spin exchange interaction constant K decreases to λ_1 = 2172 nm (for Mn^{2+} ions) and λ_2 = 2180 nm (for Mn^{3+} ions) and after that it begins to increase. The magnetic susceptibility of Mn_3O_4 has maximal value, when the intensity of applied magnetic

field is 5868 Oe. The anisotropic energy barrier decreases with the increasing of H and θ. The energy barrier increases quadratic with the increasing of H and θ. The energy of electron spin x has bigger values for Mn^{3+} ions in the case when T = 10 K. The values of energy of interaction between two electrons are bigger when T = 35 K.

Acknowledgements

The author would like to express here gratefulness to Pr. Dr. Ing. Karem Boubaker, Unité de physique des dispositifs à semi-conducteurs, Tunis EL MANAR University, Tunisia, for providing hausmannite thin films for investigation. The author would like to thank for the financial support of the project RD-08-109/08.02.2016 from Shumen University "Konstantin Preslavsky."

Author details

Petya Petkova

Address all correspondence to: petya232@abv.bg

Department of Experimental Physics, Faculty of Natural Sciences, Konstantin Preslavsky University of Shumen, Shumen, Bulgaria

References

[1] Xiao J, Yang S, Wan I, Xiao F, Wang S, J. Power Sources 245 (2014) 1027

[2] Chen W Z, Jiao Z, Wu H M, Shek H C, Wu L M C, Lai L K J, Progr. Mater. Sci. 56 (2011) 901

[3] Sanga B, Nagoyab Y, Kushiyab K, Yamase O, Sol. Energ. Mat. Sol. Cells 75 (2003) 179

[4] Fu Q, Hu L, Yu D, Sun J, Zhang H, Huo B, Zhao Z, Mater. Lett. 63 (2009) 316

[5] Shimomura T, Kim D, Nakayama M, J. Lumin. 112 (2005) 191

[6] Henley J S, Ashfold R N M, Cherns D, Surf. Coat. Technol. 177–178 (2004) 271

[7] Sasi B, Gopchandran G K, Sol. Energ. Mat. Sol. Cells 91 (2007) 1505

[8] Boukhachem A, Boughalmi R, Karyaoui M, Mhamdi A, Chtourou R, Boubaker K, Amlouk M, Mater. Sci. Eng. B 188 (2014) 72

[9] Krunks M, Soon J, Unt T, Mere A, Mikli V, Vacuum 107 (2014) 242

[10] Sharmaa R, Acharya D A, Shrivastava B S, Shripathi T, Ganesan V, Optik 125 (2014) 6751

[11] Kerli S, Alver U, Yaykaşlı H, Appl. Surf. Sci. 318 (2014) 164

[12] Boukhachem A, Kamoun O, Mrabet C, Mannai C, Zouaghi N, Yumakc A, Boubaker K, Amlouk M, Mater. Res. Bull. 72 (2015) 252

[13] Boukhachem A, Bouzidi C, Boughalmi R, Ouerteni R, Kahlaoui M, Ouni B, Elhouichet H, Amlouk M, Ceram. Int. 40 (2014) 13427

[14] Boukhachem A, Ziouche A, Ben Amor M, Kamoun O, Zergoug M, Maghraoui-Meherzi H, Yumak A, Boubaker K, Amlouk M, Mater. Res. Bull. 74 (2016) 202

[15] Arifa H, Boukhachem A, Askri B, Boubaker K, Yumak A, Raouadi K, Ceram. Int. 42 (2016) 2147

[16] Larbi T, Ouni B, Boukhachem A, Boubaker K, Amlouk M, Mater. Res. Bull. 60 (2014) 457–466

[17] Kizel A V, Krassilov I J, Burkov I V, Uspehi fizicheskih nauk 114 (1974) 295

[18] Sivaramakrishnan V, Magneto-optic study of some inorganic acids and their salts, Journal of the Indian Institute of Science. 1954

[19] Syed M, Siahmakoun A, Optical Mat. 27 (2005) 1629–1636

[20] Alwyn Scott, Encyclopedia of Nonlinear Science, Edited by Scott A, Taylor & Francis Group, New York, 2005

[21] Jönsson E P, Super paramagnetism and spin glass dynamics of interacting magnetic nanoparticle systems, Edited by Rice SA, Advances in chemical physics, Hoboken, JN: John Wiley & Sons, Inc, 2004, vol. 128, pp. 191–248

[22] Stoner C E, Wohlfarth P E, Proc. R Soc. Lond. A. 240 (1948) 599–642

[23] Speliotis E D, J. Magn. Magn. Mater. 193 (1999) 29

[24] Suzdalev P I, Suzdalev I P, Russian Chem. Rev. 70(3) (2001) 177–210

[25] Chantrell W R, Grady O K, Magnetism, Boston: Dordrecht, 1992

[26] Veynger I A, Zabrodskii G A, Tisnek V T, Phys. Technol. Semiconduct. 34 (2000) 1

IntechOpen